Published in final edited form as:
J Magn Reson Imaging. 2015 March ; 41(3): 665–675. doi:10.1002/jmri.24582.

Histological - MRI Correlation in the Primary Motor Cortex of Patients with Amyotrophic Lateral Sclerosis

Mark D. Meadowcroft, Ph.D.[1,2], **Nathan J. Mutic, M.S.**[2], **Don C. Bigler, Ph.D.**[2], **Jian-li Wang, M.D., Ph.D.**[2], **Zachary Simmons, M.D.**[3], **James R. Connor, Ph.D.**[1], and **Qing X. Yang, Ph.D.**[2]

[1]Department of Neurosurgery, The Pennsylvania State University – College of Medicine, Milton S. Hershey Medical Center, Hershey, Pennsylvania.

[2]Department of Radiology (Center for NMR Research), The Pennsylvania State University – College of Medicine, Milton S. Hershey Medical Center, Hershey, Pennsylvania.

[3]Department of Neurology, The Pennsylvania State University – College of Medicine, Milton S. Hershey Medical Center, Hershey, Pennsylvania.

Abstract

Purpose—The goal of this study was to establish the relationship between ALS histopathology and quantitative MRI metrics.

Methods—ALS patients (N=8) in advanced stages of the disease were enrolled and, immediately after death, the brain of each patient was removed. Freshly excised ALS tissue was imaged at 3.0 T with T_1 and T_2 mapping protocols and subsequently stained with astrocyte, myelin, and neuronal markers. Measures of ALS histological stains were compared to the internal control (primary visual cortex) and longitudinal parametric maps.

Results—Post-mortem T_1-weighted images demonstrate diminished contrast between gray and white matter and alterations in T_1 relaxation within the primary motor cortex. An increase in astrocyte number and reactivity as well as evident neuronal loss, a decrease in axonal density, and unraveling of the myelin sheaths in subcortical white matter were found in the ALS primary motor cortex (PMC) exhibiting significant T_1 relaxation and contrast changes.

Conclusion—This study provides a histopathological basis for differences in MR T_1 contrast and relaxation seen in the ALS brain.

Keywords

Amyotrophic lateral sclerosis; ALS; Magnetic Resonance Imaging; MRI; T1; Longitudinal Relaxation; Histology

Introduction

The progressive loss of upper motor neurons (UMN) in the motor cortex and lower motor neurons (LMN) within the spinal cord and brainstem are hallmarks of amyotrophic lateral

Corresponding Author: Mark D. Meadowcroft, Ph.D. Departments of Neurosurgery and Radiology M.S. Hershey Medical Center 500 University Drive Hershey, PA 17033 717-531-6069 markmeadowcroft@psu.edu.

sclerosis (ALS) (1, 2). Most cases occur sporadically and are of unknown etiology as the progression of cellular events in the nervous system from initial insult to final cell death is unknown. The diagnosis of ALS early in the clinical course, before the neurological examination findings are classic, may be challenging (3). A diagnosis of UMN ALS is made based upon clinical manifestation of the disease, when clinical signs appear only after neurons in the primary motor cortex (PMC) have been profoundly affected (4). The pathological events precipitating disease onset and the pattern of disease progression are not fully understood (5).

Magnetic resonance imaging (MRI) is a noninvasive technique that provides structural information on both cell loss and metabolic changes (6). However, the manner in which MRI parameters relate to the specific physical changes in the ALS brain has not been established and validated. The goal of this research was to study the relationship between post-mortem quantitative MRI and ALS histo-pathology. The aim is to develop a deeper understanding of ALS pathophysiology as viewed through non-invasive MR imaging metrics.

Methods

ALS Patients and Controls

Eight upper motor neuron ALS patients (7 male, ages 56 to 83 (mean 64.7 ± 3.7) years) were recruited with informed consent through the ALS Clinic at The Pennsylvania State University – M.S. Hershey Medical Center following institution review board approved guidelines. All ALS subjects were clinically evaluated at study entry and during subsequent patient visits with ALS-specific demographics and clinical markers of disease severity. Manual muscle testing, as measured by the Medical Research Council (MRC) scale (7), ALS Functional Rating Scale-Revised (ALSFRS-R) (8), and El Escorial ALS classification (9) were determined during patient visits. As rapidly as possible after death, the brain of each patient was removed with consent following institutional guidelines. Control tissue from the primary motor cortex of six cognitively normal subjects (4 male, ages 52 to 70 (mean 60 ± 2.5) years) was obtained from the Harvard Brain Tissue Resource Center (McLean Hospital, Belmont, MA) in a fixed state with 10% formalin following institutional guidelines. Fixed PMC control tissue samples were used for histological comparison to ALS PMC tissue. Procuring normal aged control post-mortem tissue in a fresh state for MR imaging within a timely fashion following unexpected passing was not possible in the current study. A flowchart of the methods can be seen in Fig 1.

MRI Scan

Freshly excised whole brains of ALS patients were hemi-sectioned in the midsagittal plane including the brainstem and cerebellum. The right hemisphere was rinsed in cool water and placed in an airtight cylindrical container, embedded in liquid dental alginate, and sealed to prevent tissue desiccation. The alginate was prepared immediately prior to embedding with a final mixing ratio of 50% by volume with cool distilled water (dH_2O). Upon setting, the alginate becomes an elastic solid material with high water content which aids in tissue preservation, stability to reduce settling, and acts as an anti-desiccant to maintain tissue

hydration during MR imaging without altering cortical surface transverse and longitudinal relaxation times (10, 11).

Embedded fresh ALS tissue was allowed to reach ambient room temperature (22°C) and placed in a quadrature head transmit and receive RF coil within a 3.0 T Bruker Biospin system (Ettlingen, Germany). A $3DT_1$ sequence with a TE/TR = 4.8/25.33 ms, scan matrix = 256 × 256 × 60, FOV = 200 × 200 × 60 mm, resolution = 0.78 × 0.78 × 1 mm, eight averages for a total time of 2h26m. For T_2 transverse relaxometry a spin-echo (SE) multi-slice multi-echo (MSME) T_2 scan was employed with a TE/TR = 14/5000 ms, scan matrix = 256 × 192, FOV = 200 × 200 mm, resolution = 0.78 × 1.04 mm, 3mm slice thickness, 20 slices, 14 echoes (14 – 196 ms), eight averages, flip angle = 180°, for a total time of 1h4m. For longitudinal T_1 relaxometry a MSME variable timing T_1 scan (12) was used with a TE = 14.18 ms, scan matrix = 256 × 256, FOV = 200 × 200 mm, resolution = 0.78 × 0.78 mm, 2mm slice thickness, 10 slices, 8 TR times (125, 250, 500, 1000, 2000, 3000, 4000, and 6000 ms), and three averages for a total time of 3h37m. The time constraints of the imaging sessions to scan the fresh tissue as rapidly as possible necessitated the inclusion of imaging protocols with slightly different resolutions. The slice selection of all imaging protocols was chosen to cover the entirety of the bisected sagittal neuro-imaging plane including the primary motor cortex and surrounding tissue.

MRI Analysis

After completion of the imaging protocols, the fresh ALS tissue was carefully removed from the embedding material and processed similar to the control tissue such that it was placed in low odor 10% formalin for a period of one week at 4°C, with three formalin changes, to allow full fixation of deep tissue regions. A three-dimensional surface rendering of the $3DT_1$ data for each bisected brain was created with MRIcro (University of South Carolina, Columbia, SC, USA) from the MDEFT $3DT_1$ data to facilitate the precise localization of regions of interest (ROIs) for MRI analysis and excision of these regions from the whole fixed tissue for histological evaluation. The region of affected motor cortex, as defined by the decrease between gray and white matter tissue contrast in the T_1-weighted MR images, was dissected and other regions were taken from the same sagittal image plane. A standard regime for the selection and drawing of regions of interest was utilized to account for any morphological difference between patient brain samples. The gyral region for the ROIs was clearly determined on the three dimensional surface model and the same region was selected on the two dimensional T_1 and T_2 magnitude images (Fig. 2). Gray matter regions of interest were selected to include the gyral gray matter from sulcus to sulcus. White matter ROIs were selected to include subcortical white matter under the selected gray matter region with a boundary line drawn from sulcus to sulcus. The gray matter and white matter boundary was determined by the contrast on the datasets. In the case where the boundary interface contrast was diminished, such as the ALS PMC, the magnitude images had their contrast visually enhanced to improve the delineation of gray and white matter ROIs. These regions of interest were then loaded onto the parametric relaxation maps, created from the same T_1 and T_2 data sets that were used to define the ROIs on the magnitude images, and T_1 and T_2 relaxation values obtained. Visual enhancement on the magnitude images does not alter the relaxation measures obtained from the ROIs. Relaxation rate averages for a) T_1 and b) T_2

were quantified from the variable timing T_1 and multi-echo T_2 relaxation datasets from sagittal slices, respectively. For quantitative relaxation measurements of regions of interest, T_1 and T_2 datasets were analyzed with a linear regression method (12, 13) on in-house software (qMRI, The Pennsylvania State University, Hershey, PA, USA) running on the IDL 6.1 platform (Research Systems, Inc., Boulder, CO, USA). All MRI datasets were analyzed by MM and NM (4 and 2 years experience, respectively) blinded to the clinical and histo-pathological data. Relaxation curve fits for the transverse (T_2) relaxation had the first echo image removed from the calculation to account for steady state magnetization. Longitudinal T_1 and transverse T_2 Relaxation rate ratios for were determined by dividing the gray matter T_1 (or T_2) relaxation rate by the white matter T_1 (or T_2) relaxation rate.

Specifically, neocortex gray matter and subcortical white matter regions of interest selected from the anterior prefrontal cortex (aPFC) (Brodmann area 10), premotor cortex – supplementary motor area (pMC) (Brodmann area 6), primary motor cortex (PMC) (Brodmann area 4), primary somatosensory cortex (SC) (Brodmann areas 3, 1, 2) and the primary visual cortex (PVC) (Brodmann area 17). Following imaging, ALS tissue blocks approximately 1.0 - 1.5 cm^3 in volume from the same regions of interest used for relaxation measures were dissected, paraffin embedded following traditional methods, sections cut at 12 μm on a microtome, floated, and placed on poly-L-lysine and gelatin double coated slides.

Histopathology

Myelin Staining and Densitometry—Tissue sections were deparaffinized in xylene then hydrated through multiple ethanol gradients to final dH_2O rinses. Sections were stained with filtered 0.1% Luxol Fast Blue (LFB) (14) (Luxol Fast Blue - MBS, Solvent Blue 38; in 95% ethanol with 0.5% glacial acetic acid) (S3382, Sigma-Aldrich, St. Louis, MS, USA) solution for precisely 24 hours at room temperature (maintained at 22°C). Sections were then rinsed in 95% ethanol followed by dH_2O before differentiation in 0.05% lithium carbonate (L4283, Sigma-Aldrich, St. Louis, MS, USA) (in dH_2O) solution for exactly 40 seconds. Differentiation was continued in 70% ethanol for exactly 40 seconds. Sections were then rinsed in dH_2O and counterstained with 0.1% cresyl violet solution (C1791, Sigma-Aldrich, St. Louis, MS, USA) (in dH_2O with 10 drops of glacial acetic acid immediately prior to usage) for exactly one minute, rinsed in dH_2O, dehydrated in 95% ethanol twice for five minutes followed by two five minute passes through xylene till final coverslipping according to standard procedures. Great care was taken during the differentiation stages in the lithium carbonate and 70% ethanol as the length of differentiation time influences stain saturation. As such, the differentiation time points were standardized amongst samples to allow densitometric comparison between samples. Dried slides were then scanned with a calibrated Bio-Rad GS-800 densitometer along with standards to grade the amount of differentiation for final quantification comparison. Tissue sections were stained in large batches to control for procedural variability. To confirm the lack of variation between samples, serial sections from the same tissue source were stained in different batches and were determined to have no statistical difference in optical density. Quality assurance slides were made using materials of varying opacity and used to determine precision of the densitometer and normalize measurements between batches.

Densitometer measurements were taken in gray matter and white matter regions of interest and quantified per tissue type. Quantity One 4.5 software (Bio-Rad Laboratories, Hercules, CA, USA) was used to subtract background light and measure optical density of LFB stained myelin in white matter.

Astrocyte and Neurofilament Staining—Five tissue sections from each ROI per ALS brain were deparaffinized in xylene then hydrated through graded ethanol solutions to dH_2O. Primary antibodies used were monoclonal mouse anti-glial fibrillary acidic protein (GFAP) (GA5) antibody (NCL-GFAPGA5, Novovastra - Leica Microsystems, Buffalo Grove, IL, USA) at 1:100 dilution and monoclonal anti-neurofilament 200kD (MAB377, Chemicon International, Temecula, CA, USA) at 1:500 dilution in phosphate buffered saline (PBS) diluted blocking serum. Staining was accomplished according to the manufacturers' instructions using the avidin-biotin complex peroxidase method (ABC Elite Kit, Vector Laboratories, Burlingame, CA, USA). The manufacturers' instructions were amended with an epitope retrieval step using 10 mM citrate buffer pH 6.0 at 95°C for 20 min following tissue hydration. 3, 3′-diaminobenzidine tetrahydrochloride (D4418, Sigma-Aldrich, St. Louis, MS, USA) was used as a peroxidase substrate with an incubation time of five minutes. The tissue was then rinsed in dH2O, dehydrated to xylene through graded ethanol, and coverslipped. Sections were observed on a Nikon Optiphot microscope and images were acquired with a Nikon DS-Fi1 camera and processed with Nikon Elements Imaging software.

Transmission Electron Microscopy—Fresh non-fixed ALS tissue blocks approximately 1 cm^3 of neocortex and subcortical white matter were harvested from each ROI per ALS brain and immediately placed in a 4% paraformaldehyde / 2.5% gluteraldehyde solution overnight. Regions of subcortical white matter with dimensions of approximately 1 × 1 × 3 mm were dissected from the aforementioned 1 cm^3 blocks with the extended dimension parallel to the white matter myelin bundle orientation. These small blocks were put back in fresh paraformaldehyde/gluteraldehyde fixative for two hours. The tissue was then washed three times in cold 0.1 M sodium cacodylate buffer (C4945, Sigma-Aldrich, St. Louis, MS, USA) (pH 7.4) for 10 min. This was followed by post fixation/ staining in 2% osmium tetroxide (75632, Sigma-Aldrich, St. Louis, MS, USA) buffered with 0.1 M sodium cacodylate overnight at room temperature. The tissue was then rinsed three times in cold 0.1 M sodium cacodylate buffer for 10 min each to remove the osmium tetroxide. This was followed by tissue dehydration through graded ethanol and two final 30 min dehydrations in 100% propylene oxide followed by embedding in epoxy resin. Sections were cut at 90 nm using a diamond knife microtome, perpendicular to the orientation of the white matter bundles. These sections were then transferred onto a copper grid, observed at a magnification of x7700, and photographed on a Philips TEM 400 followed by visual image assessment of myelin degradation.

Quantification of Astrocytosis and GFAP Positive Count—Gray matter, white matter, and the gray-white matter boundary were observed and scored in a blinded fashion (MM and NM, 4 and 2 years) for degree of astrocytosis and GFAP positive count on a standardized 200× imaging field. Multiple imaging fields were quantified for each slide of

each ROI per ALS and control brain. Regions were scored from one to five based on the following criteria adapted from review of previous histological quantification of astrocytosis (15); a score of one indicated few astrocytes with none displaying reactive morphology. A score of two indicated few astrocytes with some displaying reactivity (~25%). A three indicated a noticeable increase in astrocyte number with patchy distribution of reactive astrocytes (~50%). A four indicated a noticeable increase in astrocyte number with many reactive astrocytes (~75%). A five indicated a remarkable increase in astrocyte number with almost all displaying reactive morphology (~100%). Reactive astrocytes were characterized from those in a resting state by their hypertrophy, larger size, enlarged and extended processes, and increases in intermediate filaments (16, 17).

Astrocytes positive for GFAP in ALS tissue were counted in specific regions of interest. A standardized imaging field was utilized on 200× magnification images such that all images had GFAP positive astrocytes counted and averaged within this defined field. Astrocytes were considered positive if they demonstrated GFAP antibody binding in either activated, intermediate, or resting states.

Statistical Analysis

MRI relaxation measures results were statistically analyzed using an Analysis of Variance (ANOVA) and a Tukey's post-hoc for pairwise comparison within ALS ROIs in the SPSS software suite (IBM Corporation). Histological astrocyte count and densitometry metrics were analyzed with an ANOVA and post-hoc tests for comparison between ALS and control tissue and within ALS samples. An Analysis of Covariance (ANCOVA) followed by pairwise post-hoc comparison was used to test if the MRI scan delay, ALSFRS measure, and disease duration were statistical covariates within the design. With regard to the ALSFRS measurement, the inability to predict patient death required that the last patient visit ALSFRS be used in the analysis. With the nature the ALS disease course, had the ALSFRS been taken just prior to death it is logical to assume the measure would be reduced compared to the last visit. A Mann–Whitney U test was further used to determine significance in the degree of astrocytosis due to the ordinal ranking scale utilized.

Results

The mean of the patient ALS – Functional Rating Scale (ALSFRS) score at last clinical visit prior to death was 23.0 ± 2.9. The average disease duration (time between onset and death) was 27.4 ± 4.1 months. The average time between the last ALSFRS examination and time of death was 3.9 ± 1.4 months. The average MRI scan delay between tissue excision and scanning was 24 ± 14.8 hours.

A representative T_1-weighted image from the three-dimension data of an ALS cadaver brain is seen in Fig. 2a. Magnetic resonance images of freshly excised ALS cadaver brains visually show increased signal contrast (hyperintensity) in the gray matter of the PMC (anterior central gyrus), central sulcus gray matter, and samotosensory cortex (posterior central gyrus). Deep white matter shows little difference in overall contrast while anterior central gyrus subcortical white matter, especially at the white matter / gray matter boundary, shows a decrease (hypointensity) in T_1-weighted contrast. There is a lack of gray and white

matter boundary contrast within the primary motor cortex (arrow), when compared to other brain regions of ALS cadaver brains. A three dimensional surface rendering of the same $3DT_1$ data in Fig. 2a is seen in Figs. 2b and c viewed laterally and dorsally, respectively. The surface rendering clearly portrays the gyri and sulci of the ALS brain to aid in localization of region of interest for tissue dissection. The dorsal view of the rendering highlights the location of the slice selection in Fig. 2a. The slice selection exhibiting dimension T_1 contrast in the PMC is in the location of the hip, knee and trunk along the motor cortex homunculus. Manual muscle testing at the last patient clinical visit prior to death of this patient determined lower extremity involvement in the hip and knee. Region of interest selection for gray (blue) and white (red) matter in the measurement of MR T_1 and T_2 parametrics is represented in Fig. 2d. The visual contrast is reflected in the relaxation rate measurements of gray and white matter in the PMC as seen in Fig. 3. For T_1 ratios, the PMC was significantly less than all other included regions of interests ($p < 0.000$, 0.008, 0.04, and 0.05 for aPFC, pMC, SC and PVC respectively). The average T_1 rate for PMC gray matter was slightly decreased (1545 ± 58 ms; $p < 0.46$, 0.01, 0.15, and 0.40 for aPFC, pMC, SC and PVC, respectively) while a more pronounced significant increase was found in white matter (1218 ± 25 ms; $p < 0.000$, 0.10, 0.77, and 0.001 for aPFC, pMC, SC and PVC, respectively) compared to other ROIs. The resultant ratio indicates that T_1 rates for gray and white matter are approaching one another, with white matter being the dominant contributing factor. This is seen on the T_1 weighted image as a decrease in T_1 contrast in PMC gray matter, approaching that of white matter. The aPFC T_1 ratio was also significantly increased compared to the pMC, SC and PVC ($p < 0.03$, 0.004 and 0.000, respectively). Relaxation ratios for T_2 gray matter to white matter showed significant differences between the aPFC and the SC ($p < 0.02$) as well as the PVC ($p < 0.04$). No significance was observed in T_2 ratios for the PMC compared to other regions of interest. The analysis of covariance (ANCOVA) inclusion of MRI scan delay after death, final ALSFRS measure, and disease duration as covariates in the statistical design did not reduce the statistical significance of the gray, white, or gray/white matter ratio T_1 or T_2 measures ($p < 0.05$, in all cases).

Neurofilament staining for neuronal bodies and axons, GFAP staining for astrocytes, and Luxol fast blue for myelin density in the PMC are seen for both controls and ALS tissue samples in Fig. 4a at 50x, 200x and ~10× magnification, respectively. Neurofilament staining indicates that there is a decrease in neuronal body staining and reduction in the length of associated neuronal axons in ALS tissue. Astrocyte staining shows less proliferation of GFAP positive astrocytes in control tissue compared to ALS tissue. Astrocytes found in the ALS PMC show an upregulation of GFAP positive filaments. The proliferation, hypertrophy, and cellular processes associated with ALS astrocytes are indicative of a reactive state. Luxol fast blue staining of myelin is more pronounced in white matter of ALS PMC tissue, indicative of oligodendrocyte myelin sheath deterioration.

Astrocyte cell counts in gray matter, WM/GM boundary, and white matter are seen in Fig 4b. The PMC exhibits significantly more positive GFAP cells in the gray matter than the primary visual cortex ($p < 0.000$). White matter and WM/GM boundary cell counts were not significant between regions of interest. Within the primary motor cortex, gray matter had significantly more GFAP positive astrocytes than white matter ($p < 0.03$) and the WM/GM

boundary ($p < 0.028$). White matter within the primary visual cortex had significantly more astrocytes and gray matter ($p < 0.000$). Gray matter within the primary visual cortex had significantly less GFAP positive astrocytes than the WM/GM boundary ($p < 0.016$)

The degree of astrocytosis for GFAP positive astrocytes in the primary motor cortex tissue of control and ALS samples is seen in Fig. 4c. The degree of astrocytosis in gray matter was not significantly different between ALS and control PMC tissue. Both the gray/white matter boundary ($p < 0.014$) and white matter ($p < 0.003$) were significantly different with ALS tissue having more astrocytosis. Comparison of regions within the control PMC tissue show that the boundary region exhibits significantly more astrocytosis than gray matter ($p < 0.009$) and white matter ($p < 0.036$). Within ALS tissue, a comparison of regions shows that the boundary and white matter have more astrocytosis than gray matter, $p < 0.004$ and $p < 0.015$ respectively.

Quantification of Luxol fast blue myelin staining of all regions examined in ALS tissue and control primary motor cortex white matter through densitometry measurements is viewed in Fig. 5. Densitometry measures were significantly different, with the ALS PMC exhibiting more Luxol staining density than control tissue ($P < 0.000$). Regions of interest included the anterior prefrontal, premotor, primary motor, somatosensory, and primary visual cortices. The ALS Primary Motor Cortex had significantly more Luxol stain density than the anterior prefrontal ($P < 0.000$), premotor ($P < 0.000$), somatosensory ($P < 0.000$), and primary visual cortices ($P < 0.025$). For simplicity, the only regions which did not reach significance were the premotor cortex compared to the somotosencory cortex and the control PMC ($P > 0.05$).

Transmission electron microscopy images taken from ALS a) primary motor, (b) anterior prefrontal, and (c) primary visual cortices white matter are seen in Fig. 6. The myelin sheaths surrounding axons in the PMC are delaminated, unraveled, distressed, and fewer in number as compared to anterior prefrontal and primary visual cortices white matter axons.

Discussion

This study illustrates that longitudinal T_1 relaxation is altered in the ALS cadaver PMC and coincides with histological changes in neuronal milieu, cellular architecture, astrogliosis, and myelination. Neurofilament staining indicates a decrease in neurons and reduction in protruding axons in the ALS PMC, which is in agreement with previous research of selective degeneration of cortical motor neurons (18, 19). Astrocyte proliferation and reactive state are increased in the ALS tissue, also in agreement with previous research (20-24). Myelin examination reveals changes in structure which are supported by transgenic rat and ALS imaging studies (25, 26). These three factors, cellular architecture, astrogliosis, and myelination, all synergistically contribute to alterations in T_1 relaxation and T_1-weighted contrast through a relaxation component model into which water may be distributed (extracellular, cytoplasmic, and vesicular) and the state (free, structured, and bound) in which the water is bound to the surrounding tissue.

Regions of T_1 decrease have been reported in multiple diseases and are associated with brain atrophy, disability, and disease progression (27). The ALS cadaver brains exhibited an

average decrease in T_1 relaxation time within the PMC gray matter and an increase in white matter resulting in a convergence of T_1 relaxation for these regions. Alterations in T_1 have been associated with cellular architecture (fat content, protein containing fluids, proton density), macrophage infiltration (27, 28), free radicals (27, 29), myelination (30), and/or other paramagnetic substances (calcium mineralization, iron concentration, paramagnetic trace elements). Normal variation of T_1 relaxation rates and T_1 contrast across the neocortical gray and white matter does not explain the changes found in the ALS brain. In normal brain tissue, the variance in T_1 relaxation and contrast from one location of neocortical gray and white matter to another, respectively, remains small and are not significantly different (31-33).

The histology data supports cellular changes in the PMC gray matter of the ALS tissue that instigate a reduction in T_1 relaxation rate. Upper motor neuron and associated axonal loss is present in the ALS tissue. The alterations to proton relaxation and signal on MR images are due to biochemical changes that affect the magnetic field as the brain tissue undergoes structural modifications such as selective neuronal death and glial proliferation (34). With the death of neurons and increased proliferation of glial cells the neuronal milieu is considerably altered. The breakdown of dead neurons and neuronal axons releases free lipids and protein into the interstitial fluid of the surrounding tissue. Having lost the compartmentalization of these compounds, free water is able to interact with these macromolecules. As such, the proton water transiently interacts with proteins, lipids, and other macromolecules which enhance proton-lattice relaxation in the form of dissipated thermal motion of the molecules.

Astrocyte proliferation, especially reactive astrocytes characterized by hypertrophy with enlarged and extended processes and increases in intermediate filaments, also contribute to T_1 shortening. The degree of astrocytosis and astrocyte reactivity in the PMC of the ALS tissue is increased in the sub-cortical gray matter along the white-gray matter boundary compared to control tissue. The use of T_1-weighted imaging is a sensitive technique for viewing gliosis in clinical setting, however the cause for astrocyte mediated T_1 shorting is not well understood. Astrocyte specific T_1 shortening has been hypothesized to be due to two potential factors: 1) gemistocyte (reactive astrocyte) protein hydration layer shortening of T_1 relaxation (35) and 2) shortening of T_1 relaxation time could result from induced manganese superoxide dismutase (Mn-SOD) in mitochondria of the reactive astrocyte (36, 37).

Recent studies suggest that glial cells, in particular activated astrocytes, can release factors that result in motor neuron death (38). Neuronal death and gliosis are also coupled to long-lasting oxidative stress and the production of free radicals which are known to occur in the ALS brain (39, 40). Free radicals can initiate lipid peroxidation and neuronal death, contain unpaired outer shell electrons, and are paramagnetic (27), all of which result in T_1 shortening. Other explanations for this T_1-shortening effect include lipid-laden macrophages, paramagnetic substances, or cortical remyelination (27). Cortical regions undergoing myelin repair or remyelination also have associated T_1 shortening (30).

In the ALS cadaver tissue the data demonstrate that longitudinal relaxation rate is increasing in the subcortical PMC white matter. The alteration in T_1 relaxation rate is histologically related to a number of observations seen in the cadaver tissue. An increase in the number of GFAP positive astrocytes is observed in PMC subcortical gyral white matter tissue sections, although to a lesser degree than the cortical gray matter. The stage of reactive astrogliosis is notably higher in boundary and gyral white matter within the PMC compared to gray matter. The observed astrocytosis is prominent enough to account for some of the signal hypointensity seen in the motor cortex of MRIs of ALS cadaver brains; however, the dominant cause of T_1 signal alteration is hypothesized to be due to the alterations in the oligodendrocyte cellular architecture of the myelin within the white matter.

Axonal density and T_1 contrast correlation has been shown *in vivo* (41) and *ex vivo* (42) with a strong correlation to both myelin content and axonal density. An increase in longitudinal T_1 relaxation rate (hypointensity) in ALS subcortical white matter has been observed *in vivo* (43). The histological basis of the T_1-weighting associated with white matter in the neural tissue is multifaceted. In general, the proton sources in axons and myelin are based on a model where the three compartments can be expanded to extra-axonal water protons, axonal water protons, and intra-myelinic water protons (44). Lipid protons are also present in high quantities in healthy myelin as lipids account for approximately 75% of myelin composition (25). In general, the main components of the myelin sheath are lamellar sheets of lipids and proteins encasing a thin cytoplasmic region with a small boundary of extracellular space. The MR signal from water proton sources are limited to extra-axonal protons found between axonal/myelin bundles, intra-axonal protons, and protons found in the myelin sheath. This results in highly structured water protons with limited mobility and opportunities for macromolecular interaction. The high lipid composition and the organized laminar nature of healthy myelin dominate and account for its short relaxation time (intense signal) in T_1-weighted MR images.

Microscopic evaluation of subcortical ALS PMC white matter using a standard Luxol fast blue stain demonstrates substantial qualitative and quantitative differences compared to control tissue. Luxol fast blue MBS can validly be used to quantify myelination through densitometric evaluation (45-49) and evaluate myelin water content (46-49) as well as post mortem magnetic resonance evaluated abnormalities (50). The increased LFB binding seen in the ALS tissue is further explained by the transmission electron microscope data which was used to examine the sub-cellular myelin morphology of the ALS brains. Myelin lamellae separation and demyelination are observed along with fewer axons in subcortical white matter of the primary motor compared to primary visual and prefrontal cortical regions. The data suggest that the maintenance of the myelin becomes deficient, resulting in myelin pallor and lamellae separation on microscopic sections. The separation of myelin layers effectively increases the membrane surface area allowing more Luxol binding. This is evident by the increased staining and optical density of the PMC ALS samples compared to control tissue and other ALS regions sampled. The densitometry data positively trends with the T_1 relaxation rate as the increased Luxol binding (densitometry) relates to alterations in longitudinal relaxation. Myelin lamella separation results in the loss of water proton compartmentalization and shifts the bound and structured proton binding in the vicinity

towards a free water state. Data from SOD1 ALS model rats provide more evidence of myelin alterations as the these animals demonstrate a progressive decrease of total lipid content; those being cholesterol, cerebrosides, and phospolipids (25). The decrease in cholesterol can alter membrane fluidity and vascularization while a decrease in myelin proteolipid proteins alters membrane adhesion, compaction, and wrapping of axons (25). The increase in free water and decrease in lipid composition synergistically act to increase the longitudinal relaxation rate.

While the study has outlined a number of possibilities for the cause of the ALS gray and white matter T_1 relaxation rates, it is of considerable interest that the longitudinal relaxation (T_1) proved to be more sensitive than the transverse (T_2) relaxation in detecting differences within the regions selected. The hypothesized explanation for this is multifaceted and relates to the composition of white and gray matter brain tissue. Previous study has shown that T_1 variations in cortical gray or white matter are not statistically significant across the normal brain (31, 33). In contrast, there are statistical regional differences in T_2 found across the brain (31, 51). T_1 relaxation is known to be more sensitive than T_2 in discriminating changes in myelination and discerning between white and gray matter predominately due to lipid-water interactions of myelin (51). This study revealed subtle yet insignificant T_2 relaxation changes in white and gray matter ROIs with increased variability in the measures. T_1 relaxation is produced predominantly by the spin-lattice interaction at the lipid-water interface in white matter, which is seven-fold greater than that caused by the protein-water interface (51). For example, T_1 relaxation has provided direct measure of neonatal brain maturation as white matter myelination is dynamically occurring during the first postnatal year (52-55). Maturation changes related to brain myelination were seen earlier on T_1- than on T_2-weighted images. A similar trend to the current ALS data is found where alterations in T_1 relaxation are found to be more prominent than those of T_2 relaxation. Our histology data showed marked myelin sheet disruption in these brain areas.

The interpretations above should be considered in the context of potential study limitations. First, our results provide pathological insight into T_1 relaxation change in ALS by imaging of freshly excised ALS cadaver brain tissue and histological analyses of the same brain tissue. Ultimately, further validation is needed by *in vivo* imaging of an ALS cohort with follow-up *ex vivo* imaging and histological analysis at post mortem. Second, availability of tissue samples for post-mortem analysis was limited by variations of the length of time between clinical onset and death. Further study with a larger cohort of patients both ante-mortem (longitudinally) and post-mortem will be required to determine if the MRI metrics are related to ALS disease progression and the disease severity (ALSFRS). Thirdly, although great care was taken to minimize the time between death and tissue harvesting, further minimizing this time frame will be coordinated in future studies. Minimizing the time between death and *ex vivo* MRI of fresh tissue increases the reliability of post-mortem MRI metrics to *in vivo* conditions. Fourthly, other MR imaging modalities sensitive to detecting white matter abnormalities were not undertaken in the current study. Diffusion and magnetization transfer based methods should be considered in future studies. Lastly, freshly excised whole control brain samples were not able to be obtained in the current study. The difficulties associated with obtaining normal control tissue in a fresh state required the

utilization of tissue from the ALS primary visual cortex as an internal control for the MRI and histological metrics of the primary motor cortex. Furthermore, the visual cortex has been shown through histologic and MR measures to remain unaffected during the disease process and comparable to normal age-matched control tissue (56). While the anterior prefrontal cortex was also selected as an internal control initially, there is MR spectroscopic and morphometric evidence to support the involvement of the frontal lobe region in the disease process (57, 58). In addition, as the control tissue samples were obtained in a previously formalin fixed state; MR images were not able to be obtained from the control tissue to compare to the MR metrics from the fresh non-fixed ALS tissue. Future study with the inclusion of freshly excised control tissue is needed to verify and substantiate the differences outlined in this study.

The data demonstrated that longitudinal MRI relaxation is sensitive to histological metrics of ALS tissue, and that MR images of freshly excised ALS cadaver brains have alterations in gray and white matter T_1 contrast within the PMC when compared to unaffected brain regions. The overall trend is a slight decrease in T_1 relaxation rate (hyperintensity) in the gray matter and a dominant increase in T_1 relaxation rate (hypointensity) in white matter. The histology analyses revealed quantifiable differences between ALS affected and unaffected tissue. These results provided pathological basis of the MR contrast and relaxation changes in the ALS cadaver brains. The gray matter decrease in T_1 relaxation is hypothesized to be due to causative factors such as the 1) immobilization of water molecules due to macromolecular hydration or surface relaxation caused by the released proteins through cellular degradation, 2) advanced neural gliosis, and 3) paramagnetic relaxation associated with free radical production. The increase in T_1 relaxation seen in white matter is hypothesized to be due to 1) an increase in water proton motility, 2) decrease in proton compartmentalization due to myelin destabilization, 3) and a decrease in total lipid content. The T_1 alterations in ALS warrants further study as a potential clinically relevant biomarker of the disease progression.

Acknowledgements

Funding for this project has been made available in part through the NIH (R01-AG027771-01A2), the Neuroimaging Research Grant, the Zimmerman Family Love Fund, the Paul and Harriett Campbell ALS Research Fund, the Greater Philadelphia Chapter of the ALS Association, and the Pennsylvania Department of Health using Tobacco Settlement Funds.

We would especially like to thank the ALS patients who graciously donated tissue for this study upon bereavement and their caregivers who sacrificed their time to participate.

Grant Support: NIH (R01-AG027771-01A2), the Neuroimaging Research Grant, the Zimmerman Family Love Fund, the Paul and Harriett Campbell ALS Research Fund, the Greater Philadelphia Chapter of the ALS Association, and the Pennsylvania Department of Health using Tobacco Settlement Funds.

References

1. Charil A, Corbo M, Filippi M, Kesavadas C, Agosta F, Munerati E, et al. Structural and metabolic changes in the brain of patients with upper motor neuron disorders: a multiparametric MRI study. Amyotroph Lateral Scler. Oct-Dec;2009 10(5-6):269–79. [PubMed: 19922113]
2. Hong YH, Lee KW, Sung JJ, Chang KH, Song IC. Diffusion tensor MRI as a diagnostic tool of upper motor neuron involvement in amyotrophic lateral sclerosis. J Neurol Sci. Dec 15; 2004 227(1):73–8. [PubMed: 15546594]

3. Williams TL. Motor neurone disease: diagnostic pitfalls. Clin Med. [Review]. Feb; 2013 13(1):97–100.

4. Abe O, Yamada H, Masutani Y, Aoki S, Kunimatsu A, Yamasue H, et al. Amyotrophic lateral sclerosis: diffusion tensor tractography and voxel-based analysis. NMR Biomed. Oct; 2004 17(6): 411–6. [PubMed: 15386625]

5. Veyrat-Durebex C, Corcia P, Dangoumau A, Laumonnier F, Piver E, Gordon PH, et al. Advances in Cellular Models to Explore the Pathophysiology of Amyotrophic Lateral Sclerosis. Mol Neurobiol. Nov 7.2013

6. Andjus PR, Bataveljic D, Vanhoutte G, Mitrecic D, Pizzolante F, Djogo N, et al. In vivo morphological changes in animal models of amyotrophic lateral sclerosis and Alzheimer's-like disease: MRI approach. Anat Rec (Hoboken). Dec; 2009 292(12):1882–92. [PubMed: 19943341]

7. Paternostro-Sluga T, Grim-Stieger M, Posch M, Schuhfried O, Vacariu G, Mittermaier C, et al. Reliability and validity of the Medical Research Council (MRC) scale and a modified scale for testing muscle strength in patients with radial palsy. J Rehabil Med. Aug; 2008 40(8):665–71. [PubMed: 19020701]

8. Cedarbaum JM, Stambler N, Malta E, Fuller C, Hilt D, Thurmond B, et al. The ALSFRS-R: a revised ALS functional rating scale that incorporates assessments of respiratory function. BDNF ALS Study Group (Phase III). J Neurol Sci. Oct 31; 1999 169(1-2):13–21. [PubMed: 10540002]

9. Brooks BR, Miller RG, Swash M, Munsat TL. El Escorial revisited: revised criteria for the diagnosis of amyotrophic lateral sclerosis. Amyotroph Lateral Scler Other Motor Neuron Disord. Dec; 2000 1(5):293–9. [PubMed: 11464847]

10. Bjarkam CR, Pedersen M, Sorensen JC. New strategies for embedding, orientation and sectioning of small brain specimens enable direct correlation to MR-images, brain atlases, or use of unbiased stereology. Journal of neuroscience methods. Jul 30; 2001 108(2):153–9. [Research Support, Non-U.S. Gov't]. [PubMed: 11478974]

11. Fabich HT, Vogt SJ, Sherick ML, Seymour JD, Brown JR, Franklin MJ, et al. Microbial and algal alginate gelation characterized by magnetic resonance. J Biotechnol. Oct 31; 2012 161(3):320–7. [Research Support, N.I.H., Extramural Research Support, Non-U.S. Gov't Research Support, U.S. Gov't, Non-P.H.S.]. [PubMed: 22728394]

12. Riederer SJ, Bobman SA, Lee JN, Farzaneh F, Wang HZ. Improved precision in calculated T1 MR images using multiple spin-echo acquisition. J Comput Assist Tomogr. Jan-Feb;1986 10(1):103–10. [Research Support, Non-U.S. Gov't Research Support, U.S. Gov't, P.H.S.]. [PubMed: 3944292]

13. Gupta RK. A new look at the method of variable nutation angle for the measurement of spin-lattice relaxation times using fourier transform NMR. Journal of Magnetic Resonance. 1977; 25(1):231–5.

14. Kluver H, Barrera E. A method for the combined staining of cells and fibers in the nervous system. J Neuropathol Exp Neurol. Oct; 1953 12(4):400–3. [PubMed: 13097193]

15. Ostergaard PJ, Jensen MB. Histological quantification of astrocytosis after cerebral infarction: a systematic review. Int J Neurosci. Jul; 2013 123(7):439–43. [Research Support, N.I.H., Extramural]. [PubMed: 23311713]

16. Anderson MA, Ao Y, Sofroniew MV. Heterogeneity of reactive astrocytes. Neuroscience letters. Dec 19.2013

17. Sun D, Jakobs TC. Structural remodeling of astrocytes in the injured CNS. Neuroscientist. Dec; 2012 18(6):567–88. [Research Support, N.I.H., Extramural Research Support, Non-U.S. Gov't Review]. [PubMed: 21982954]

18. Holmes G. The pathology of amyotrophic lateral sclerosis. Rev Neurol Psychiatry. 1909; 4:693–724.

19. Davison C. Amyotrophic Lateral Sclerosis: Origin and extent of the upper motor neuron lesion. Arch Neurol Psychiatry. Dec 1; 1941 46(6):1039–56. 1941.

20. Kushner PD, Stephenson DT, Wright S. Reactive astrogliosis is widespread in the subcortical white matter of amyotrophic lateral sclerosis brain. J Neuropathol Exp Neurol. May; 1991 50(3): 263–77. [PubMed: 2022968]

21. Kamo H, Haebara H, Akiguchi I, Kameyama M, Kimura H, McGeer PL. A distinctive distribution of reactive astroglia in the precentral cortex in amyotrophic lateral sclerosis. Acta Neuropathol. 1987; 74(1):33–8. [PubMed: 3310502]
22. Murayama S, Inoue K, Kawakami H, Bouldin TW, Suzuki K. A unique pattern of astrocytosis in the primary motor area in amyotrophic lateral sclerosis. Acta Neuropathol. 1991; 82(6):456–61. [PubMed: 1785258]
23. Barbeito LH, Pehar M, Cassina P, Vargas MR, Peluffo H, Viera L, et al. A role for astrocytes in motor neuron loss in amyotrophic lateral sclerosis. Brain Res Brain Res Rev. Dec; 2004 47(1-3): 263–74. [PubMed: 15572176]
24. Lasiene J, Yamanaka K. Glial cells in amyotrophic lateral sclerosis. Neurol Res Int. 2011:718987. [PubMed: 21766027]
25. Niebroj-Dobosz I, Rafalowska J, Fidzianska A, Gadamski R, Grieb P. Myelin composition of spinal cord in a model of amyotrophic lateral sclerosis (ALS) in SOD1G93A transgenic rats. Folia Neuropathol. 2007; 45(4):236–41. [PubMed: 18176898]
26. Kolind S, Sharma R, Knight S, Johansen-Berg H, Talbot K, Turner MR. Myelin imaging in amyotrophic and primary lateral sclerosis. Amyotroph Lateral Scler Frontotemporal Degener. May 16.2013
27. Janardhan V, Suri S, Bakshi R. Multiple sclerosis: hyperintense lesions in the brain on nonenhanced T1-weighted MR images evidenced as areas of T1 shortening. Radiology. Sep; 2007 244(3):823–31. [PubMed: 17690319]
28. Haimes AB, Zimmerman RD, Morgello S, Weingarten K, Becker RD, Jennis R, et al. MR imaging of brain abscesses. AJR Am J Roentgenol. May; 1989 152(5):1073–85. [PubMed: 2705342]
29. de Kerviler E, Cuenod CA, Clement O, Halimi P, Frija G, Frija J. [What is bright on T1 MRI scans?]. J Radiol. Feb; 1998 79(2):117–26. [PubMed: 9757228]
30. Terada H, Barkovich AJ, Edwards MS, Ciricillo SM. Evolution of high-intensity basal ganglia lesions on T1-weighted MR in neurofibromatosis type 1. AJNR Am J Neuroradiol. Apr; 1996 17(4):755–60. [PubMed: 8730197]
31. Wansapura JP, Holland SK, Dunn RS, Ball WS Jr. NMR relaxation times in the human brain at 3.0 tesla. J Magn Reson Imaging. Apr; 1999 9(4):531–8. [PubMed: 10232510]
32. Jezzard P, Duewell S, Balaban RS. MR relaxation times in human brain: measurement at 4 T. Radiology. Jun; 1996 199(3):773–9. [Research Support, Non-U.S. Gov't]. [PubMed: 8638004]
33. Fischer HW, Rinck PA, Van Haverbeke Y, Muller RN. Nuclear relaxation of human brain gray and white matter: analysis of field dependence and implications for MRI. Magnetic resonance in medicine : official journal of the Society of Magnetic Resonance in Medicine / Society of Magnetic Resonance in Medicine. Nov; 1990 16(2):317–34. [Research Support, Non-U.S. Gov't].
34. Fujioka M, Taoka T, Matsuo Y, Hiramatsu KI, Sakaki T. Novel brain ischemic change on MRI. Delayed ischemic hyperintensity on T1-weighted images and selective neuronal death in the caudoputamen of rats after brief focal ischemia. Stroke. May; 1999 30(5):1043–6. [PubMed: 10229742]
35. Baheti NN, Cherian A, Wattamwar PR, Kesavadas C, Thomas B. Ischemic hyperintensities on T1-weighted magnetic resonance imaging of patients with stroke: new insights from susceptibility weighted imaging. Neurol India. Jan-Feb;2010 58(1):90–4. [PubMed: 20228471]
36. Shan DE. Delayed ischemic hyperintensity of T1-weighted MRI. Stroke. Mar; 2000 31(3):797–8. [PubMed: 10700524]
37. Fujioka M, Taoka T, Matsuo Y, Hiramatsu K-I, Kondo Y, Ogoshi K, et al. Delayed ischemic hyperintensity on T1 weighted MRI and induced manganese superoxide dismutase in mitochondria after mild focal ischemia: long-lasting oxidative stress hypothesis. Stroke. 2000; 31:341.
38. Keller AF, Gravel M, Kriz J. Live imaging of amyotrophic lateral sclerosis pathogenesis: disease onset is characterized by marked induction of GFAP in Schwann cells. Glia. Aug 1; 2009 57(10): 1130–42. [PubMed: 19115383]
39. Liu D. The roles of free radicals in amyotrophic lateral sclerosis. J Mol Neurosci. 1996 Fall;7(3): 159–67. [PubMed: 8906612]

40. Liu D, Wen J, Liu J, Li L. The roles of free radicals in amyotrophic lateral sclerosis: reactive oxygen species and elevated oxidation of protein, DNA, and membrane phospholipids. FASEB J. Dec; 1999 13(15):2318–28. [PubMed: 10593879]
41. van Waesberghe JH, Kamphorst W, De Groot CJ, van Walderveen MA, Castelijns JA, Ravid R, et al. Axonal loss in multiple sclerosis lesions: magnetic resonance imaging insights into substrates of disability. Ann Neurol. Nov; 1999 46(5):747–54. [PubMed: 10553992]
42. Schmierer K, Scaravilli F, Altmann DR, Barker GJ, Miller DH. Magnetization transfer ratio and myelin in postmortem multiple sclerosis brain. Ann Neurol. Sep; 2004 56(3):407–15. [PubMed: 15349868]
43. da Rocha AJ, Oliveira AS, Fonseca RB, Maia AC Jr. Buainain RP, Lederman HM. Detection of corticospinal tract compromise in amyotrophic lateral sclerosis with brain MR imaging: relevance of the T1-weighted spin-echo magnetization transfer contrast sequence. AJNR Am J Neuroradiol. Oct; 2004 25(9):1509–15. [PubMed: 15502129]
44. Menon RS, Rusinko MS, Allen PS. Proton relaxation studies of water compartmentalization in a model neurological system. Magn Reson Med. Dec; 1992 28(2):264–74. [PubMed: 1281258]
45. Scholtz CL. Quantitative histochemistry of myelin using Luxol Fast Blue MBS. Histochem J. Nov; 1977 9(6):759–65. [PubMed: 72743]
46. Laule C, Kozlowski P, Leung E, Li DK, Mackay AL, Moore GR. Myelin water imaging of multiple sclerosis at 7 T: correlations with histopathology. Neuroimage. May 1; 2008 40(4):1575–80. [PubMed: 18321730]
47. Laule C, Leung E, Lis DK, Traboulsee AL, Paty DW, MacKay AL, et al. Myelin water imaging in multiple sclerosis: quantitative correlations with histopathology. Mult Scler. Dec; 2006 12(6):747–53. [PubMed: 17263002]
48. Laule C, Vavasour IM, Kolind SH, Li DK, Traboulsee TL, Moore GR, et al. Magnetic resonance imaging of myelin. Neurotherapeutics. Jul; 2007 4(3):460–84. [PubMed: 17599712]
49. Moore GR, Leung E, MacKay AL, Vavasour IM, Whittall KP, Cover KS, et al. A pathology-MRI study of the short-T2 component in formalin-fixed multiple sclerosis brain. Neurology. Nov 28; 2000 55(10):1506–10. [PubMed: 11094105]
50. Nijeholt GJ, Bergers E, Kamphorst W, Bot J, Nicolay K, Castelijns JA, et al. Post mortem high-resolution MRI of the spinal cord in multiple sclerosis: a correlative study with conventional MRI, histopathology and clinical phenotype. Brain. Jan; 2001 124(Pt 1):154–66. [PubMed: 11133795]
51. Koenig SH, Brown RD 3rd, Spiller M, Lundbom N. Relaxometry of brain: why white matter appears bright in MRI. Magnetic resonance in medicine : official journal of the Society of Magnetic Resonance in Medicine / Society of Magnetic Resonance in Medicine. Jun; 1990 14(3): 482–95. [Research Support, Non-U.S. Gov't].
52. Barkovich AJ, Kjos BO, Jackson DE Jr. Norman D. Normal maturation of the neonatal and infant brain: MR imaging at 1.5 T. Radiology. Jan; 1988 166(1 Pt 1):173–80. [PubMed: 3336675]
53. Masumura M. Proton relaxation time of immature brain. II. In vivo measurement of proton relaxation time (T1 and T2) in pediatric brain by MRI. Childs Nerv Syst. 1987; 3(1):6–11. [Case Reports]. [PubMed: 3594473]
54. Holland BA, Haas DK, Norman D, Brant-Zawadzki M, Newton TH. MRI of normal brain maturation. AJNR American journal of neuroradiology. Mar-Apr;1986 7(2):201–8. [PubMed: 3082150]
55. Deoni SC, Mercure E, Blasi A, Gasston D, Thomson A, Johnson M, et al. Mapping infant brain myelination with magnetic resonance imaging. J Neurosci. Jan 12; 2011 31(2):784–91. [PubMed: 21228187]
56. Lee Y, Morrison BM, Li Y, Lengacher S, Farah MH, Hoffman PN, et al. Oligodendroglia metabolically support axons and contribute to neurodegeneration. Nature. Jul 26; 2012 487(7408): 443–8. [Research Support, N.I.H., Extramural Research Support, Non-U.S. Gov't]. [PubMed: 22801498]
57. Usman U, Choi C, Camicioli R, Seres P, Lynch M, Sekhon R, et al. Mesial prefrontal cortex degeneration in amyotrophic lateral sclerosis: a high-field proton MR spectroscopy study. AJNR American journal of neuroradiology. Oct; 2011 32(9):1677–80. [Controlled Clinical Trial Research Support, Non-U.S. Gov't]. [PubMed: 21778247]

58. Cosottini M, Cecchi P, Piazza S, Pesaresi I, Fabbri S, Diciotti S, et al. Mapping Cortical Degeneration in ALS with Magnetization Transfer Ratio and Voxel-Based Morphometry. PloS one. 2013; 8(7):e68279. [PubMed: 23874570]

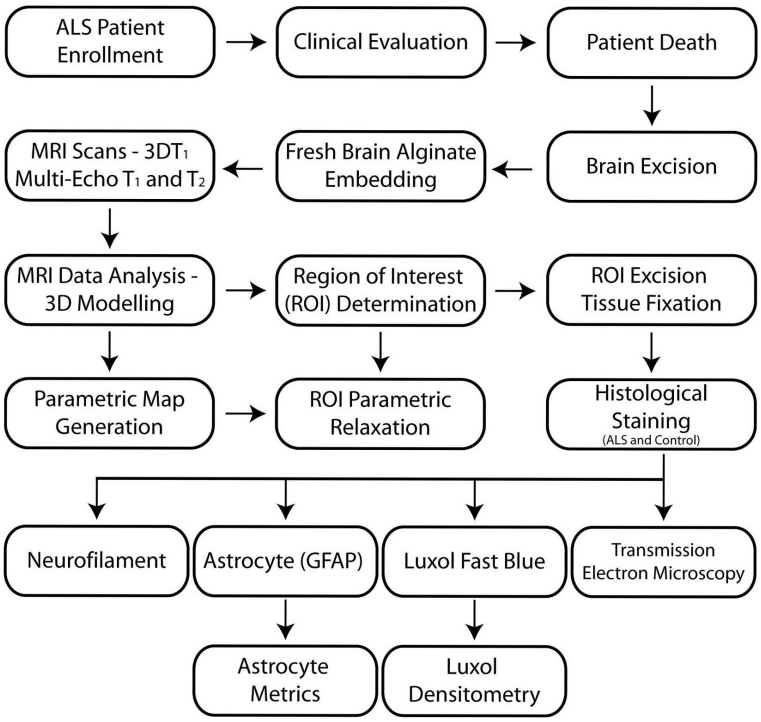

Figure 1.
Flow-chart outlining the methods utilized in the study.

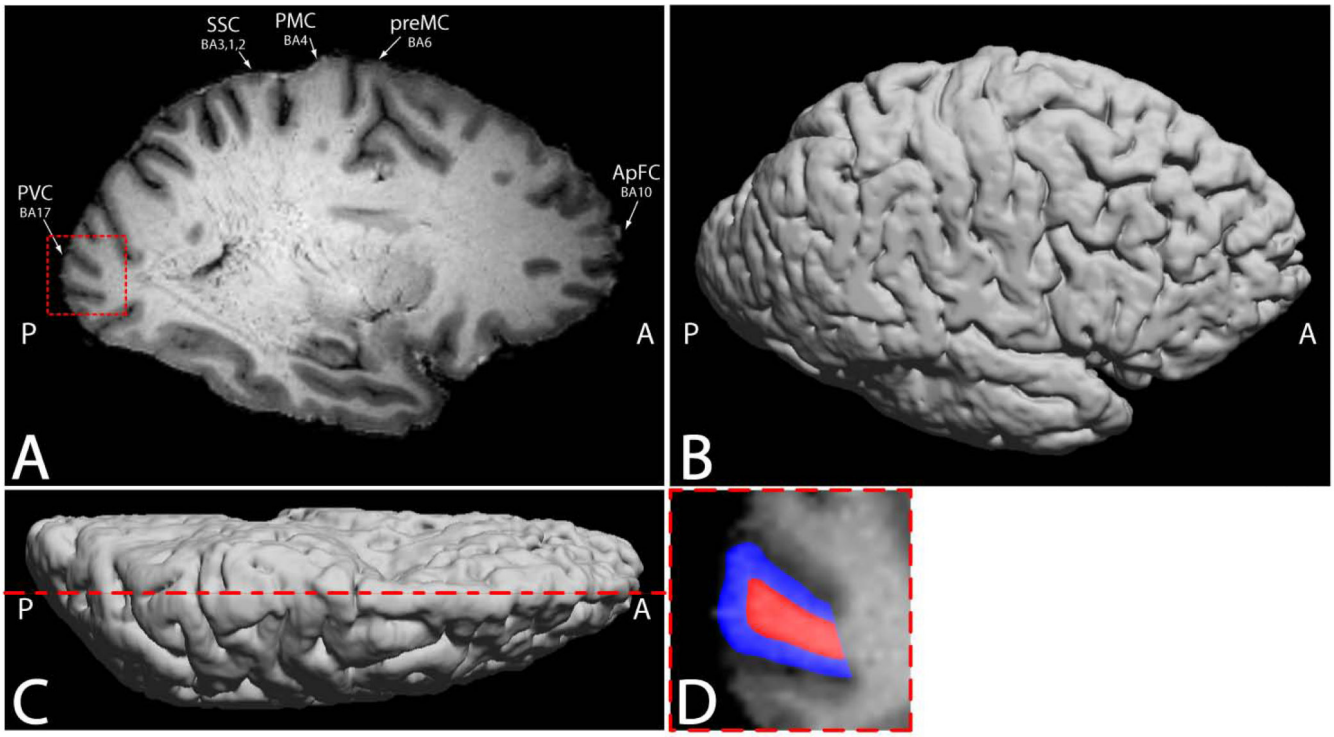

Figure 2.

a) Representative T_1-weighted image from a MDEFT $3DT_1$ scan of an ALS cadaver brain. The primary visual cortex (PVC), somatosensory cortex (SSC), primary motor cortex (PMC), premotor cortex (preMC), and anterior prefrontal cortex (ApFC) regions of interest locations are shown. The decrease in gray matter T_1 contrast and gray/white matter boundary contrast is visible in the PMC compared to other brain regions. b) Lateral view of the three dimensional surface rendering of the same $3DT_1$ data used to facilitate region of interest location for histological dissection. c) Dorsal view of the three dimensional surface rendering of the same $3DT_1$ data highlighting the location of the slice selection in (a). d) The square region emphasized in the PVC in 1a is enlarged in 1d and representative selections of gray (blue) and white (red) matter region of interests used in parametric relaxometry analysis are highlighted.

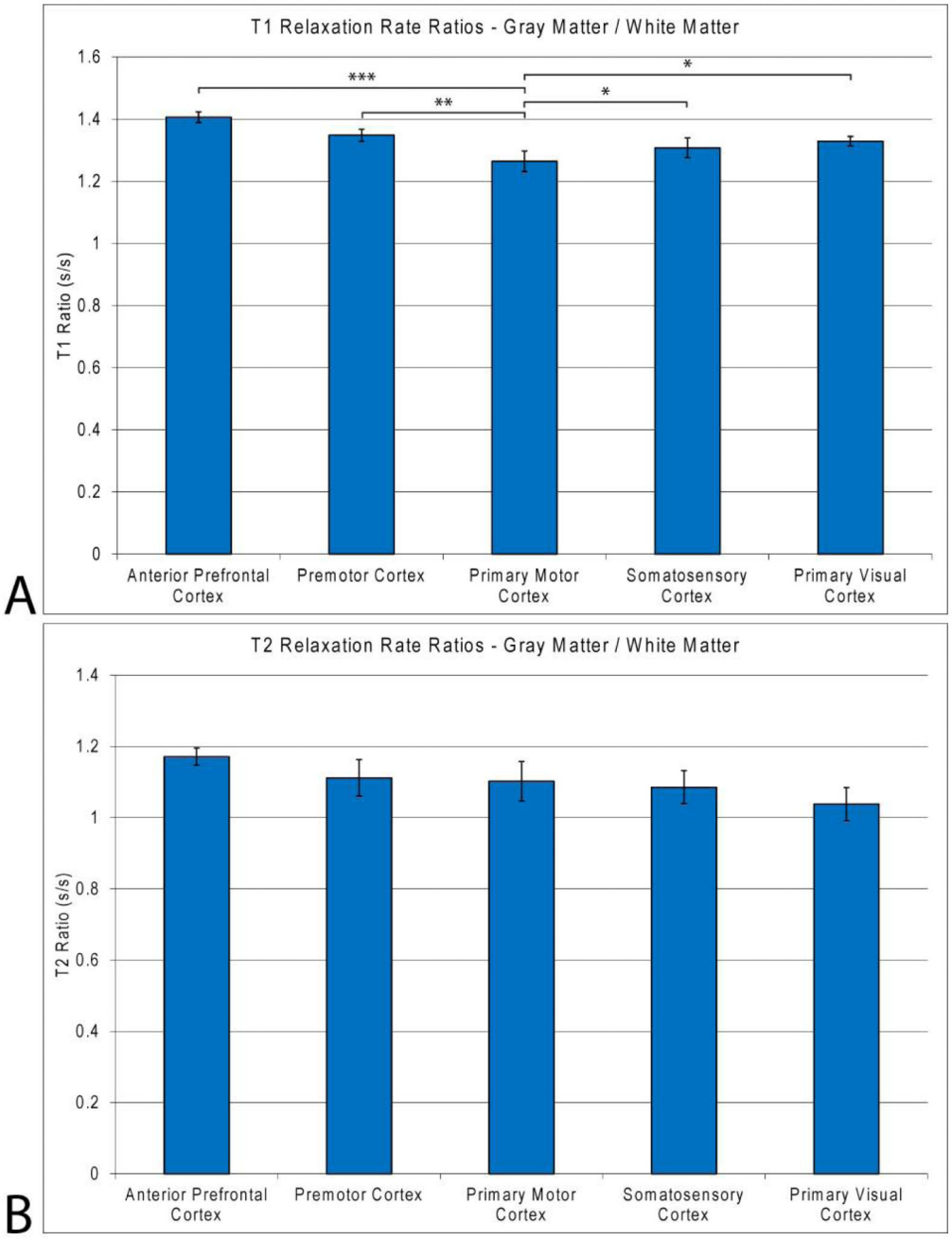

Figure 3.

a) Gray matter to white matter (a) T_1 and (b) T_2 rate ratios in ALS cadaver brain regions of interest for gray and white matter in the anterior prefrontal, premotor, primary motor, somatosensory, and primary visual cortices. PMC T_1 relaxation ratios for gray : white matter are significantly decreased compared to all other regions indicating a decrease in gray matter T_1 relaxation approaching that of white matter. The average T_2 relaxation ratios for gray : white matter do not show the same trend as the T_1 data, with no significant difference

between the PMC and regions sampled. Only significance of regions compared to PMC tissue is shown. *, $p < 0.05$; ** $p < 0.01$;, *** $p < 0.001$; **** $p < 0.0001$.

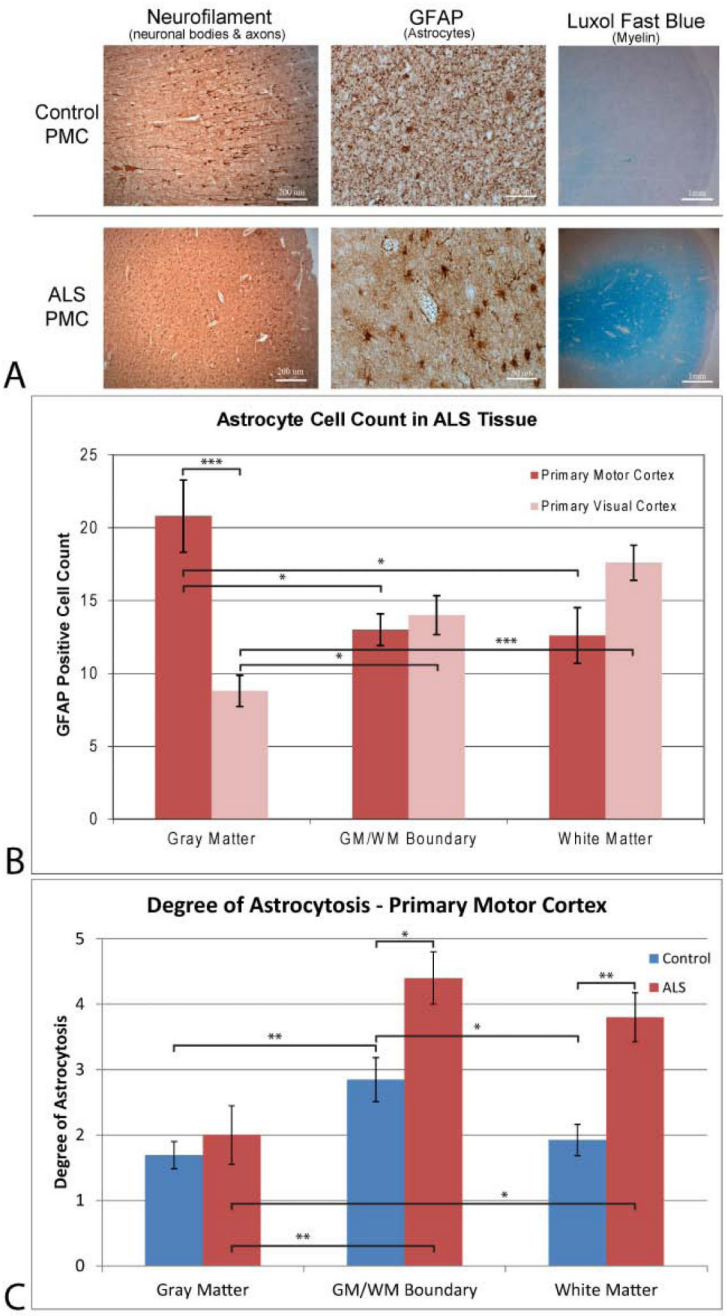

Figure 4.

– a) Histology stains, b) GFAP cell counts, and c) Degree of astrocytosis in ALS and control tissue samples. a) Antibody staining for neurons in gray matter (left – neurofilament), astrocytes in white matter (right - GFAP) and myelin (right - Luxol Fast blue) for control (top) and ALS (bottom) primary motor cortex tissue sections. Images were taken at 50x, 200x, and ~10x for the neurofilament, GFAP and Luxol stains, respectively, with scale bars at 200 μm, 50 μm, and 1mm. Neurofilament staining indicate that there is a decrease in neuronal body staining and reduction in protruding axons in ALS tissue. Astrocyte staining

shows less proliferation of GFAP positive astrocytes in control tissue compared to ALS tissue. Astrocytes found in the ALS PMC show an upregulation of GFAP positive filaments indicative of a reactive state. Luxol fast blue staining of myelin is more pronounced in white matter of ALS PMC tissue, indicative of oligodendrocyte myelin sheath deterioration. b) GFAP cell counts of the ALS primary motor and primary visual cortices. A significant increase in GFAP positive astrocytes is found within the gray matter of the ALS PMC compared to ALS primary visual cortex internal control tissue as well as white matter and white/gray boundary ALS PMC tissue. c) Degree of astrocytosis for GFAP positive astrocytes in control and ALS tissue samples in the primary motor cortex. ALS PMC tissue exhibited significantly more astrocytosis in white matter and the gray/white matter boundary than control tissue. This increase in reactive astrocytosis was not seen in the gray matter of the PMC. *, $p < 0.05$; ** $p < 0.01$;, *** $p < 0.001$; **** $p < 0.0001$.

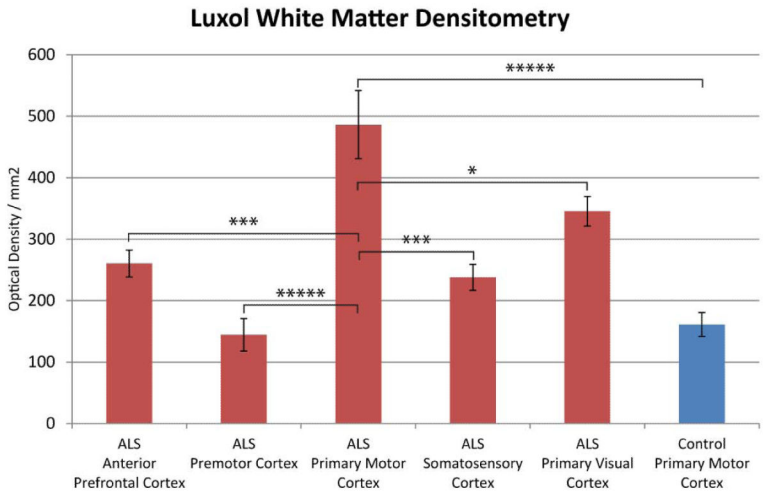

Figure 5.

Luxol fast blue densitometry measurements of ALS and control primary motor cortex white matter and across the ALS cadaver tissue regions. The ALS PMC exhibited significantly more luxol staining than all regions sampled. For simplicity, only significance is shown for the ALS PMC compared to all other regions. *, $p < 0.05$; ** $p < 0.01$; *** $p < 0.001$; **** $p < 0.0001$; ***** $P < 0.00001$.

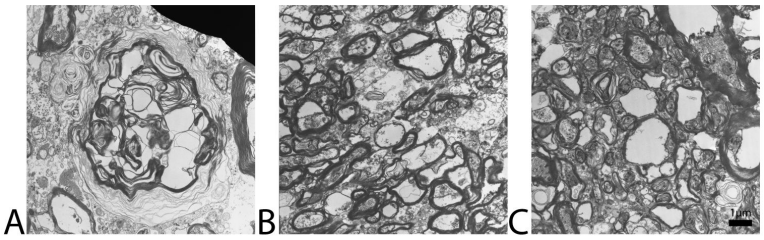

Figure 6.

Transmission electron microscopy images taken from ALS a) primary motor, (b) anterior prefrontal, and (c) primary visual cortices. Images were taken at a magnification of x7700 for all tissues. The myelin sheaths surrounding axons in the PMC are delaminated and unraveled as compared to anterior prefrontal and primary visual cortices axons. Scale bar has been calibrated to 1 μm in length.